

# Chapter 7

## Graphene-Based Ultra-Broadband Slow-Light System and Plasmonic Whispering-Gallery-Mode Nanoresonators

Weibin Qiu

**Abstract** In this chapter, the graphene monolayer is modeled as surface current density without thickness in order to explore the properties of the plasmons propagating along it. The proposed model is verified analytically in terms of the propagation constant of the plasmons. By using this zero-thickness model, the nanofocusing properties of the mid infrared electromagnetic wave and the slow-light system of infrared wave are investigated. A focus width of 1.6 nm for a wavelength of 56 THz is achieved on a gradient chemical potential distribution graphene. Variant frequency components of the plasmons are stopped at the different locations of the gradient chemical potential distributed graphene monolayer forming “rainbow” capture effect. Additionally, the tunable whispering-gallery mode properties of the graphene monolayer coated semiconductor nanowire are also studied. An effective mode area smaller than  $3.75 \times 10^{-5}(\lambda_0)^2$ , and a quality factor of 195 are obtained in a nanowire with a diameter of 5 nm. The proposed model and the plasmonic structures may find broad implications in the fields of high density plasmonic integrated circuits technique and transformation plasmonics.

**Keywords** Graphene • Plasmon • Zero-thickness • Nanofocusing • Slow light • Whispering-Gallery Mode

### 7.1 Introduction

Graphene, a 2-dimensional (2D) material composed of a single carbon atom layer, has caught intensive research since it was discovered. This awesome material offers promising fantastic applications in electronic and photonic devices [1–5], metamaterials [6], optical cloaking [7], femtosecond lasers [8], nonlinear optics [9], and solar cells [10], due to its unique zero-gap band structure with linear dispersion relation, In a suitable range of chemical potential and photon frequency,

---

W. Qiu (✉)

College of Information Science and Engineering, Huaqiao University, Xiamen, China

e-mail: [wbiqiu@hqu.edu.cn](mailto:wbiqiu@hqu.edu.cn)

graphene behaves like a semi-metallic material and consequently is able to support surface plasmonic polariton (SPP) wave [11]. Furthermore, comparing with noble materials, graphene supported SPP waves possess outstanding advantages, such as relatively low loss, high confinement, and most significantly, and tunability [12]. This application of graphene in the field of plasmonics includes sensors [13], nanoribbon waveguides [14, 15], resonators [16], splitters [17], filter [18, 19], polarization convertor [20], modulators [21], and antenna [22, 23]. Also, peculiar optical behaviors such as slow light system [24], and anomalous reflection [25] of the graphene supported SPP have been reported. The propagation of SPP wave along the graphene sheet can be tailored by modifying the chemical potential. Thus, graphene offers another freedom to engineer the SPP wave without any geometric engineering. In this chapter, by using the finite element method (FEM) technique, the nanofocusing of MIR on a graphene monolayer which has spatially gradient chemical potential without complicated device geometry is numerically analyzed. In addition, the dynamic group velocity and tunable rainbow capture and relieving of plasmons along graphene sheet is discussed. Also, the optical properties of the graphene monolayer-coated dielectric nanowire resonators are discussed.

This chapter is organized as the following, besides the introduction section, the validity of the zero-thickness graphene monolayer model is reviewed analytically in the second section. In Sect. 7.3, the surface conductivity of graphene is discussed in terms of the chemical potential. The propagation constant of the plasmon along graphene is discussed in the Sect. 7.4. Nanofocusing properties of the MIR EM field are reviewed in the Sect. 7.5. Later on, the dynamic group velocity control and rainbow capture and relieving mechanism of plasmon along graphene sheet is discussed in the Sect. 7.6. In the Sect. 7.7, the tunable WGM properties of the graphene monolayer coated dielectric nanowire resonator are discussed (Fig. 7.1).

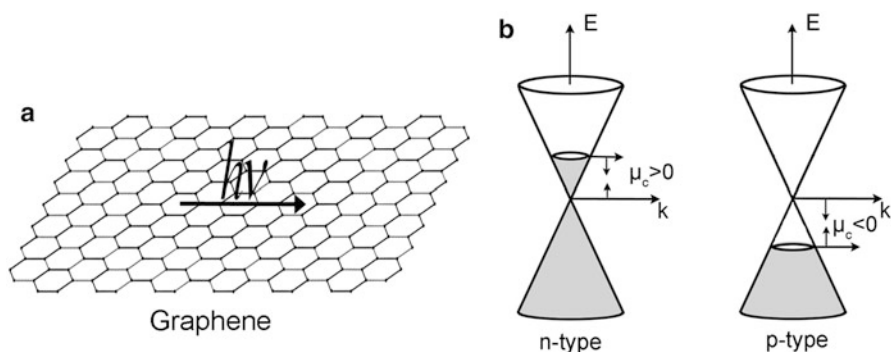


**Fig. 7.1** The schematic molecule structure and energy band structure of graphene monolayer

## 7.2 Validity of the Zero-Thickness Graphene Monolayer Model

Among most of the literatures, the graphene monolayer sheet was modeled as a metallic layer with a finite “effective thickness”  $d_{eff}$ , where the corresponding “effective dielectric constant”  $\epsilon_{eff}(d_{eff})$ . Then the thin layer was treated similarly to the noble metal materials. The dispersion relation, i.e. the propagation constant as a function of the frequency, is obtained from the common three-layer planar waveguide system. They also demonstrated that when the effective thickness below certain value, the dispersion relation kept unchanged. However, it should be pointed out that the concept of dielectric constant is based on bulk materials. Nevertheless, graphene is composed of a single layer of carbon atom. Substantially, it is not a bulk material, and of course, it is unsuitable to use the concept of dielectric constant. The similar case is the concept of temperature, one cannot define a temperature of a molecule, or a finite number of molecules.

In order to avoid the embarrassment described above, the concepts of “effective thickness” and “effective dielectric constant” should be abandoned. Alternatively a concise model is adapted, where the graphene monolayer is treated as a conductive layer without thickness. So it is characterized by surface conductivity  $\sigma$ . It could be shown that dispersion relation got from the proposed model is identical that got from the “effective thickness” model when the “effective thickness” approaches to zero.

The graphene ultra-thin film is supposed with a thickness  $\Delta = a$ . And it is characterized by an equivalent permittivity of  $\epsilon_{g,eq}(\Delta)$ , which is dependent upon the thickness  $\Delta$ .

$$\epsilon_{g,eq} = 1 + \frac{i\sigma_g \eta_0}{k_0 \Delta} \tag{7.1}$$

In Fig. 7.2a, the graphene sheet is located on ZOY plane and the plasmon propagates along z direction.

Only the TM polarized SPPs supported by graphene is considered. Assume the EM field propagates along the y-axis. Since the graphene sheet is infinite in y direction,  $\frac{\partial}{\partial y} \rightarrow 0$ , the non-zero components of the TM polarization are  $(E_y, E_z, H_x)$ ,

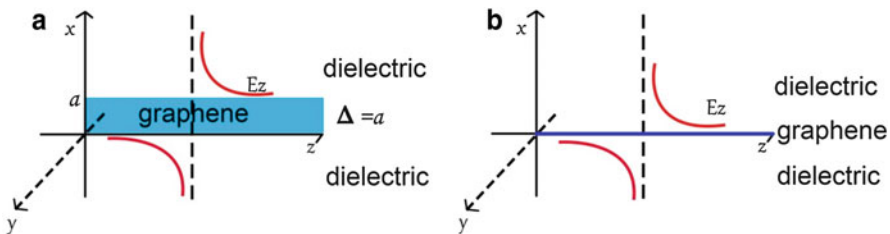


**Fig. 7.2** The schematic diagram of (a) three layers non-zero thickness model (b) zero-thickness model of graphene monolayer

According to the traditional waveguide theory, the electric field in the different regions can be written as

$$E_x = \begin{cases} Ae^{-k_h(x-a)} \exp(i(\omega t - \beta z)) & (x > a) \\ (Be^{k_g(x-a)} + Ce^{-k_g x}) \exp(i(\omega t - \beta z)) & (0 < x < a) \\ De^{k_h(x+b)} \exp(i(\omega t - \beta z)) & (x < 0) \end{cases} \quad (7.2)$$

Where A-D are unsolved mode amplitudes,  $k_h = (\beta^2 - \varepsilon_h k_0^2)^{1/2}$ ,  $k_g = (\beta^2 - \varepsilon_{g,eq} k_0^2)^{1/2}$ ,  $\beta$  is the propagation constant.  $\varepsilon_h$  is the relative permittivity of the free space.

$$\begin{cases} H_y = \frac{\omega \varepsilon}{\beta} E_x \\ E_z = -\frac{j}{\omega \varepsilon} \frac{\partial H_y}{\partial x} \end{cases} \rightarrow E_z = -\frac{j}{\beta} \frac{\partial E_x}{\partial x}$$

and

$$E_y = H_x = H_z = 0$$

For the different regions,

$$\begin{cases} z > a \\ \begin{cases} E_x = Ae^{-k_h(x-a)} \\ H_y = \frac{\omega \varepsilon_r \varepsilon_0}{\beta} Ae^{-k_h(x-a)} \\ E_z = \frac{i}{\beta} k_h Ae^{-k_h(x-a)} \end{cases} \end{cases} \quad \begin{cases} 0 < z < a \\ \begin{cases} E_x = Be^{k_g(x-a)} + Ce^{-k_g x} \\ H_y = \frac{\omega \varepsilon_g \varepsilon_0}{\beta} (Be^{k_g(x-a)} + Ce^{-k_g x}) \\ E_z = -\frac{i}{\beta} k_g (Be^{k_g(x-a)} - Ce^{-k_g x}) \end{cases} \end{cases} \quad \begin{cases} z < 0 \\ \begin{cases} E_x = De^{-k_h x} \\ H_y = \frac{\omega \varepsilon_r \varepsilon_0}{\beta} De^{-k_h x} \\ E_z = -\frac{i}{\beta} k_h De^{-k_h x} \end{cases} \end{cases} \quad (7.3)$$

Take the boundary conditions into account,

$$\begin{aligned} z = a & \quad z = 0 \\ \begin{cases} A\varepsilon_r = \varepsilon_g(B + Ce^{-k_g a}) \\ Ak_h = -k_g(B - Ce^{-k_g a}) \end{cases} & \quad \begin{cases} \varepsilon_g(Be^{-k_g a} + C) = \varepsilon_r D \\ k_g(Be^{-k_g a} - C) = k_h D \end{cases} \end{aligned} \quad (7.4)$$

$$\begin{cases} \varepsilon_{g,eq} = 1 + \frac{i\sigma_g \eta_0}{k_0 \Delta} \\ k_h = (\beta^2 - \varepsilon_h k_0^2)^{1/2} \\ k_g = (\beta^2 - \varepsilon_{g,eq} k_0^2)^{1/2} \end{cases} \quad (7.5)$$

$$\text{then } k_h = -\frac{\varepsilon_h}{1 + \frac{i\sigma_g \eta_0}{k_0 a}} \frac{2}{a}$$

When  $a \rightarrow 0$ ,

$$k_h = -\frac{2\varepsilon_h k_0}{i\sigma_g \eta_0} \quad (7.6)$$

substitute Eqs. (7.6, 7.5), the propagation constant (wave vector) of the SPPs is given by

$$k_{SPP} = k_g = k_0 \sqrt{\varepsilon_h - \left(\frac{2\varepsilon_h}{\sigma_g \eta_0}\right)^2} \quad (7.7)$$

When it comes to the zero-thickness model, the graphene sheet also locates on the surface of YOZ, and the plasmon propagates along  $z$  direction. Also, only TM mode is considered. The non-zero components of the EM field are identical with the non-zero-model. The whole space is divided into two parts,  $z > 0$ , and  $z < 0$ . The non-zero components of the EM fields in the different regions are written as

$$E_x = \begin{cases} A \exp(-k_h x) \exp(i(\omega t - \beta z)) & x > 0 \\ B \exp(k_h x) \exp(i(\omega t - \beta z)) & x < 0 \end{cases}$$

According to Maxwell's equations  $\nabla \times H = \frac{\partial D}{\partial t} = \varepsilon_0 \varepsilon_r \frac{\partial E}{\partial t}$  and  $\begin{cases} \frac{\partial H_y}{\partial x} = \varepsilon_0 \varepsilon_r \frac{\partial E_z}{\partial t} \\ E_x = \frac{\beta}{\omega \varepsilon_0 \varepsilon_r} H_y \end{cases}$  we can get  $H_y$ ,  $E_z$  in different regions. Here, one can ignore  $\exp(i(\omega t - \beta z))$ .

$$\begin{cases} x > 0 \\ H_y = \frac{\beta}{\omega \varepsilon_0 \varepsilon_r} A \exp(-k_h x) \\ E_z = \frac{i\beta}{(\omega \varepsilon_0 \varepsilon_r)^2} k_h A \exp(-k_h x) \end{cases} \quad \begin{cases} x < 0 \\ H_y = \frac{\beta}{\omega \varepsilon_0 \varepsilon_r} B \exp(-k_h x) \\ E_z = -\frac{i\beta}{(\omega \varepsilon_0 \varepsilon_r)^2} k_h B \exp(-k_h x) \end{cases} \quad (7.8)$$

Where A-B are unsolved mode amplitudes which can be eliminated.  $k_1$  and  $k_2$  is wave vector of the dielectric in the different regions,  $\beta$  is the propagation constant.  $\varepsilon_r$  is the relative permittivity.  $\omega$  is the angular frequency.

$$k_h = (\beta^2 - \omega^2 \varepsilon_0 \varepsilon_r \mu_0)^{1/2} = (\beta^2 - \varepsilon_r k_0^2)^{1/2} \quad (7.9)$$

According to the boundary conditions

$$\begin{cases} \lim_{x \rightarrow 0^+} H_y - \lim_{x \rightarrow 0^-} H_y = J_s \\ J_s = \sigma_g E_z(x=0) \\ E_z(x=0) = \lim_{x \rightarrow 0^-} E_z = \lim_{x \rightarrow 0^+} E_z \end{cases}$$

Where  $\sigma_g$  is the surface conductivity.

A, B,  $k_1$  and  $k_2$  can be solved by solving the boundary equation,

$$\begin{cases} A = -B \\ k_1 = k_2 = \frac{2\omega\epsilon_0\epsilon_r}{i\sigma_g} \end{cases}$$

Substitute them to Eq. (7.11), the propagation constant can be got

$$\beta = \frac{\omega}{c} \sqrt{\epsilon_r - \frac{4\epsilon_r^2\epsilon_0}{\mu_0\sigma_g^2}} \quad (7.10)$$

Where vacuum wave impedance  $\eta_0 = \sqrt{\frac{\mu_0}{\epsilon_0}}$  and  $k_0 = \frac{\omega}{c}$ , the propagation constant  $\beta$  can be written as

$$\beta = k_0 \sqrt{\epsilon_r - \frac{4\epsilon_r^2}{\eta_0\sigma_g^2}} \quad (7.11)$$

So, the validity of the zero-thickness is conformed. It is the limit condition when the effective thickness approaches to 0.

### 7.3 Surface Conductivity of Graphene

Graphene's surface conductivity  $\sigma_g$  is composed of the contribution from interband electron transition  $\sigma_{inter}$  and intraband electron-photon scattering  $\sigma_{intra}$ ,  $\sigma_g = \sigma_{inter} + \sigma_{intra}$ , According to Kubo formula,

$$\sigma_{inter} = i \frac{e^2}{4\pi\hbar} \ln \left[ \frac{2|\mu_c| - \hbar(\varpi + i\tau^{-1})}{2|\mu_c| + \hbar(\varpi + i\tau^{-1})} \right], \quad (7.12)$$

$$\sigma_{intra} = i \frac{e^2 k_B T}{\pi \hbar^2 (\varpi + i\tau^{-1})} \left[ \frac{\mu_c}{k_B T} + 2 \ln \left( \exp \left( -\frac{\mu_c}{k_B T} + 1 \right) \right) \right] \quad (7.13)$$

Where  $\omega$  is the angular frequency of the plasmon,  $\tau$  is the electron momentum relaxation time. Experimental works demonstrated that more than 2 eV of chemical potential [26] and more 3 ps [27] of relaxation time have been achieved. Here the adapted chemical potential is less than 1.3 eV and the relaxation time is less than 1.4 ps. So it is conservative enough to ignore the additional damping channels due to the plasmon-phonon interaction [28]. Figure 7.3 reveals the schematic of the interband transitions and intraband scattering.

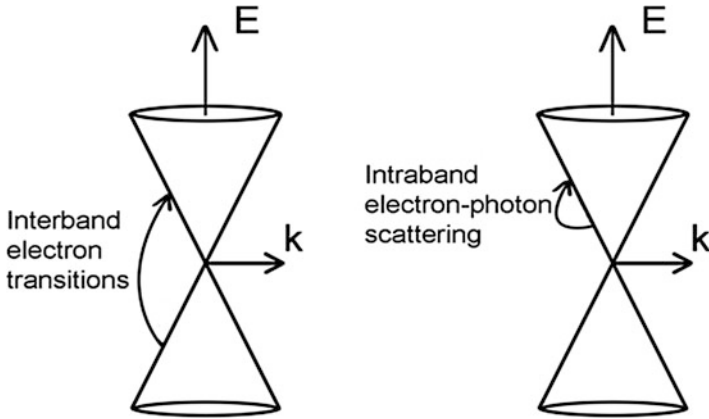


**Fig. 7.3** The schematic diagram of interband electron transitions and intraband electron-photon scattering

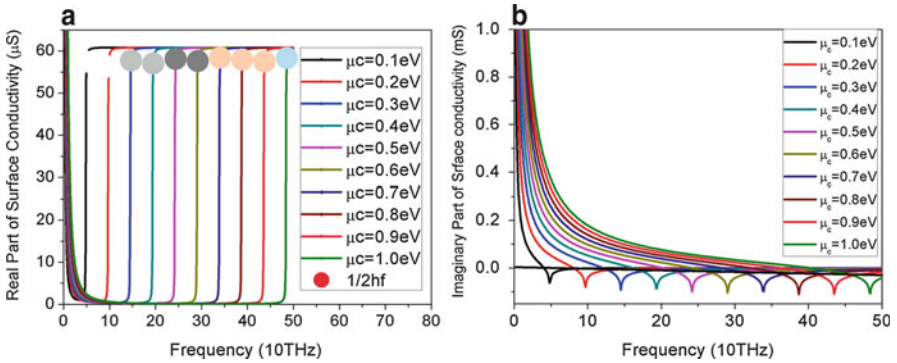


**Fig. 7.4** The real and imaginary parts of the surface conductivity of graphene as a function of photon frequency with respect to various chemical potentials. (a) real parts, (b) imaginary parts

Furthermore,  $\sigma_g$  can be rewritten as  $\sigma_g = \sigma'_g + i\sigma''_g$ , Fig. 7.4a demonstrate the real and imaginary parts of surface conductivity as function of frequency respective to various chemical potentials. SPP wave can be supported when  $\sigma''_g > 0$ , while the real part of the conductivity  $\sigma'_g$  denotes the absorption loss of the SPP wave on graphene sheet. In Fig. 7.4b, some special points are highlighted, which correspond to the relation  $\mu_c = 1/2\hbar\omega$ . when  $\mu_c < 1/2\hbar\omega$ ,  $\sigma'_g$  is stable at  $60.5 \mu\text{S}$ , which is substantially high and constrains the propagation distance of the SPP wave. When  $\mu_c > 1/2\hbar\omega$ ,  $\sigma'_g$  is low and ensures the long propagation distance of the SPP. Interestingly, when  $1/2\hbar\omega$  approaches to  $\mu_c$ ,  $\sigma'_g$  reduces and even becomes negative when  $\mu_c$  is very close to  $1/2\hbar\omega$ , where TM SPP is no longer supported. Albeit TE surface mode might be supported when  $\sigma''_g < 0$ , it suffers high

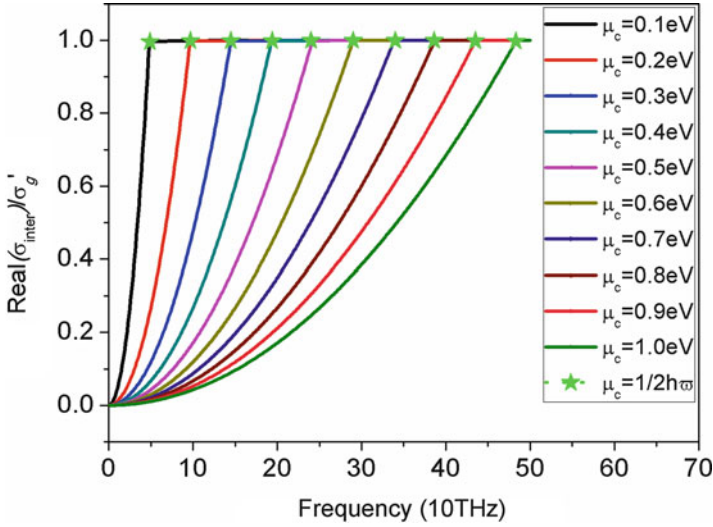


**Fig. 7.5** Percentage of the contribution from interband electron transitions on the total surface conductivity as a function of the photon frequency with respect to various chemical potentials

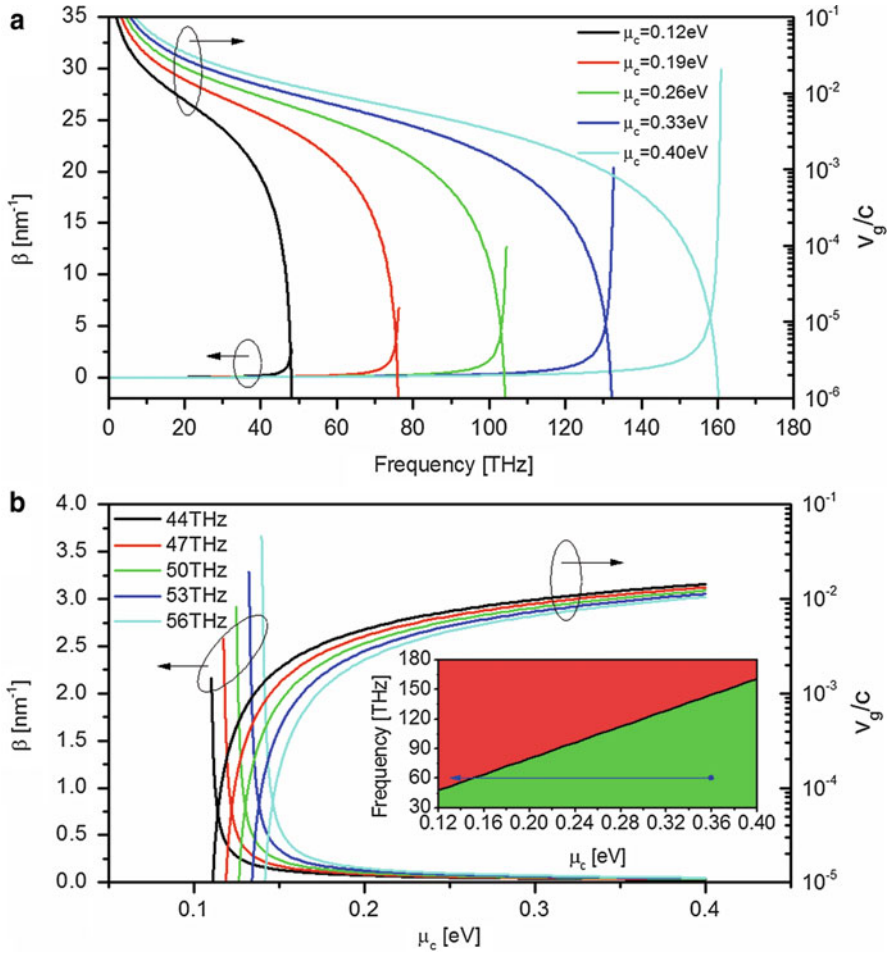
absorption loss due to the high  $\sigma_g'$  value at this region. So  $\mu_c = 1/2\hbar\omega$  is very close to the critical point of the graphene supported TM SPP wave.

Figure 7.5 reveals the ratio between the real part of  $\sigma_{inter}$  and the real part of the total surface conductivity  $\sigma_g$  as a function frequency with respect to various chemical potentials. In addition, the points corresponding to  $\mu_c = 1/2\hbar\omega$  are highlighted. For a given chemical potential, in the low frequency region, the contribution from electron interband transition is low, which means the propagation loss is high. Moreover, when  $1/2\hbar\omega$  approaches to  $\mu_c$  the contribution grows as the increasing of the frequency, corresponding to a weaker contribution from intraband electron-photon scattering. Particularly, More than 99 % percent of the total surface conductivity comes the contribution from interband electron transition when  $\mu_c < 1/2\hbar\omega$ . So,  $\mu_c = 1/2\hbar\omega$  is the critical point not only for the absolute value of the surface conductivity, and also for the contribution ratio for different mechanisms.

## 7.4 Analysis of the Propagation Constant of the Plasmons Along the Graphene Monolayer

When the plasmons propagate along an infinite graphene monolayer sheet with a uniform chemical potential  $\mu_c$ , the dispersion relation is given by Eq. (7.13). In more detail, the propagation constant  $\beta$  is rewritten by  $\beta = \beta' + \beta''$ , The wavenumber  $\beta'$  and the group velocity of SPP waves on graphene sheet with spatially homogeneous  $\mu_c$  are shown in Fig. 7.6a as a function of frequency  $f$ .





**Fig. 7.6** (a) The dispersion relation and group velocity of SPP waves propagating along free-standing graphene with homogeneous chemical potential. (b) The wavenumber and group velocity of SPP waves as a function of chemical potential. The inset in (b) shows the critical frequency as a function of chemical potential. The *green regime* indicates that SPP waves are allowed and the *red regime* indicates the SPP waves are fully damped or not supported. For each chemical potential, calculation is not performed for frequencies higher than its critical frequency

Here we define that for a certain chemical potential, the critical frequency  $f_c$  is the frequency that gives equal real part and imaginary part of the complex wavenumber, i.e.  $\beta' = \beta''$ . In other words, the SPP wave is fully damped. The curve of the inset of Fig. 7.6b shows critical frequency corresponding to different chemical potentials. As the frequency approaches the critical frequency  $f_c$  for a certain chemical potential,  $\beta'$  increases drastically. Since  $2\pi/\beta'$  is the wavelength of the SPP wave and implies the spatial extension of EM waves, the confinement of the EM waves along graphene is very strong and nanofocusing effect is expected around this frequency  $f_c$ . For example, the critical frequencies for chemical

potentials of 0.12 and 0.40 eV are 48.1 and 160.9 THz, respectively. Furthermore, around critical frequency, the group velocity  $v_g$  becomes very low. Ideally if  $\beta'$  goes to infinite as the frequency increases, zero group velocity of the SPP wave would be achieved and the wavelength of the SPP wave would shrink to zero as well, which means that the EM field is concentrated on a singularity point on the graphene sheet. Of course, there is loss accompanying wave propagation and such ideal case is hardly achievable.

## 7.5 Nanofocusing of the Mid Infrared Electromagnetic Field on the Gradient Chemical Potential Distributed Graphene Monolayer

Similar behavior will occur when the frequency is kept fixed and the chemical potential is gradually reduced, which means that the SPP wave of a certain frequency propagate along a graphene sheet with spatially decreasing gradient chemical potential. This scenario is indicated by the blue trajectory in the inset of Fig. 7.2b. The green regime means  $\beta' > \beta''$  and the red regime means  $\beta' < \beta''$  or SPP waves are not supported. As the chemical potential decreases,  $\beta'$  becomes larger, the confinement of the light field becomes stronger, and the group velocity slows down. Together with the slowing down of group velocity, the intensity accumulates and becomes increasingly higher, which is essentially a result of energy conservation. As the point follows the trajectory and approaches the red regime in the inset of Fig. 7.6b, the chemical potential goes sufficiently low and the loss of the SPP waves becomes higher and higher at the same time. Therefore, nanofocusing effect actually depends on the competition between energy accumulation and loss during propagation. As long as the energy accumulation rate far exceeds energy loss rate, nanofocusing effect can be expected. Additionally, if the incident wave is composed of several frequency components, different frequencies would be focused at different positions on a graphene sheet with appropriately designed chemical potential distribution.

To numerically verify the discussion above, Finite element method simulation is used COMSOL Multiphysics to compute the light field of SPP waves propagating along a graphene monolayer with gradient chemical potential  $\mu_c$ . The graphene sheet is in the XOZ plane at  $y = 250$  nm and SPP waves are launched at  $x = 0$  nm. The distribution of chemical potential  $\mu_c$  over the graphene sheet is a function of position. In the simulation, it is defined to be

$$\mu_c = \mu_{c0}[1 - \exp(0.015(x - 1000))] \quad (7.14)$$

where  $\mu_{c0} = 0.4\text{eV}$  is the chemical potential at  $x = 0$  nm. The purpose of choosing this distribution is nothing more than having a spatially rapidly varied chemical potential. The frequencies of simulated SPP waves are 44, 47, 50, 53, and 56 THz.

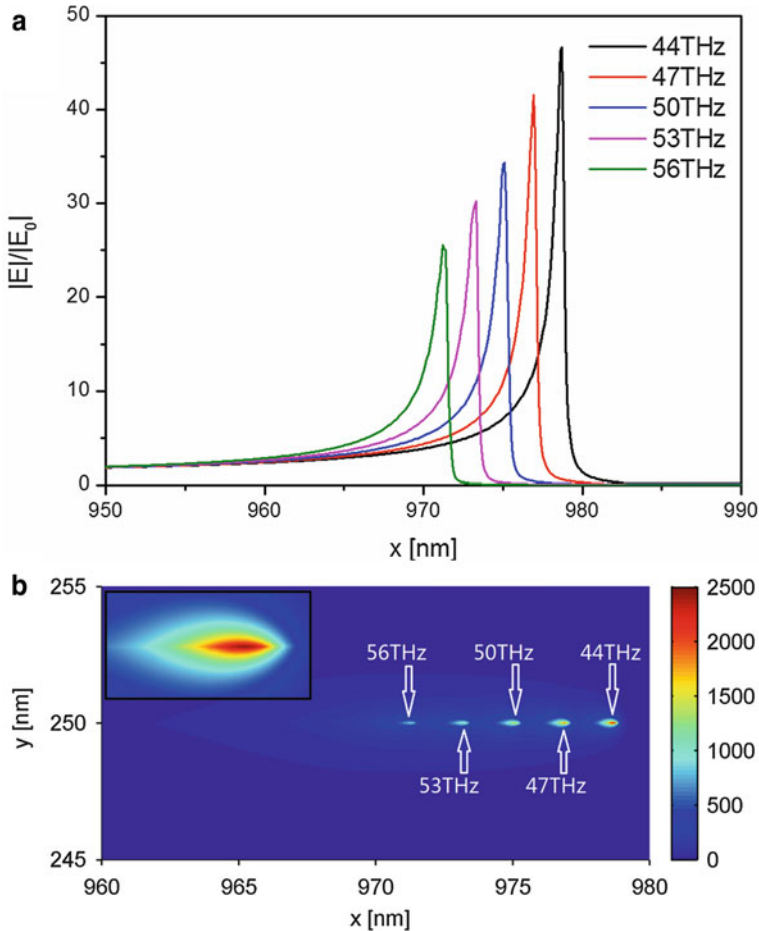


**Fig. 7.7** (a) The evolution of electric field norm around the focusing spots along the graphene sheet at  $y = 250$  nm. The values are normalized by the electric field norm at the launching point. (b) The time averaged energy density distribution near the focusing spots. The values are normalized by the time averaged energy density at the launching point. If five frequencies are launched together, they will be focused at different positions. The inset in (b) is a magnification of the focusing spot of 44 THz

The corresponding wavelength in free space is 6.81, 6.38, 6.00, 5.66, and 5.35  $\mu\text{m}$ . The evolution of  $|\mathbf{E}|$  during propagation at  $y = 250$  nm, i.e. along the graphene sheet, is shown in Fig. 7.7a and the values have been normalized with the norm of electric field at the launching point  $|\mathbf{E}_0|$ . The intensity enhancement factor  $R = |\mathbf{E}_{\text{peak}}|^2/|\mathbf{E}_0|^2$  reaches 654 for 56 THz and even 2178 for 44 THz. The full width at half maximum (FWHM) of the focusing spot of 56 THz is 1.6 nm. It is obvious that other frequencies have spot size on the same order, which indicates that nanofocusing effect is achieved for different frequencies on the same structure.

The five distinct focusing spots of the frequencies are clearly shown in Fig. 7.7b, where the time averaged energy density of each frequency is normalized by the time averaged energy density at the launching point. Since the position of the focusing spot depends on the chemical potential distribution, it can be tuned by modifying the distribution of chemical potential. Meanwhile the intensity enhancement factor  $R$  might be changed consequently as well. Passing the focusing spot, the SPP waves vanish due to EM loss [29]. Before SPP waves reach the focusing spot, the local chemical potential is far above  $\hbar\omega/2$ ,  $\sigma_{\text{inter}}$  has a small real part and the loss is dominated by intraband electron-photon scattering, thereby bringing very limited loss to the propagation of SPP waves. However, when the chemical potential continues decreasing and reaches around  $\hbar\omega/2$ , the contribution of loss from interband electron transition indicated by Eqs. (7.14) and (7.15) becomes more significant and eventually dwarfs the counterpart from intraband electron-photon scattering, resulting the SPP waves to disappear. In a way similar to defining critical frequency, the critical chemical potential  $\mu_c$  for a certain frequency can be defined as the chemical potential that gives  $\beta' = \beta''$ . It is worthwhile to point out that the position of the focusing point is determined by the location of the critical  $\mu_c$ , while the size of the focusing point is fully controlled by how rapidly  $\mu_c$  approaches the critical value. Practically, one should keep the chemical potential far from the threshold to avoid propagation loss and then reduce it to the critical value as rapidly as possible at desired position to get nanofocusing. In our chemical potential distribution governed by Eq. (7.16), the group velocity remains almost unchanged before the chemical potential falls down rapidly. Take 56 THz as an example. At the FWHM of the focusing spot, the group velocity finally drastically slows down to  $5 \times 10^{-5}$  times the light speed in vacuum, effectively enabling energy accumulation in the vicinity of the focusing spot.

## 7.6 Ultra-Broadband Rainbow Capture and Releasing Along Gradient Chemical Potential Distributed Graphene Monolayer

In order to dynamically control the group velocity of the plasmon, one can consider a graphene sheet where the chemical potential gradually decreases along the SPP wave propagation direction. From the analysis of Sect. 7.4, it is already known that the group velocity of a wave with radian frequency  $\omega$  will be trapped at the position where the critical condition discussed above is satisfied. Furthermore, different frequencies would be trapped at different positions on the gradient chemical potential graphene. This actually means broadband light trapping. In contrast to the nanofocusing effect, it does require the chemical potential decreasing abruptly. The above arguments can be verified by simulation based on COMSOL multiphysics Finite Element Method (FEM). In the simulation, the length of the

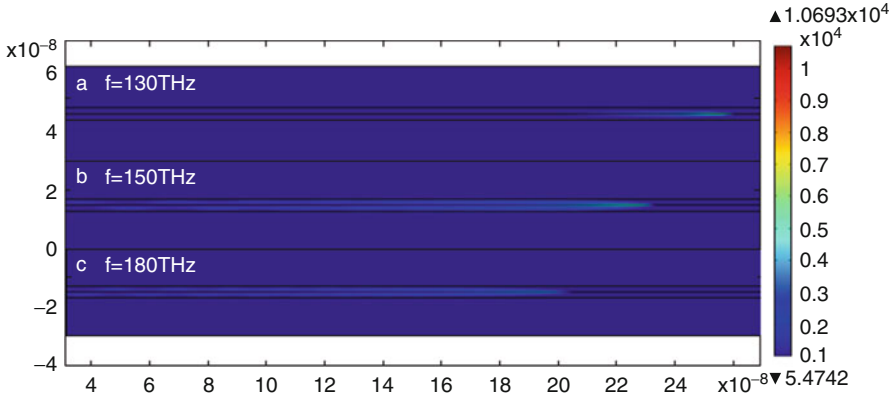


**Fig. 7.8** The  $|E|$  field distribution of 130, 150, and 180 THz plasmons along the graphene sheet whose chemical potential is governed by  $\mu_{c0}(x)$ . The 130, 150, and 180 THz plasmons are trapped at 279.45, 231 and 200.5 nm, respectively

graphene sheet is 300 nm. The chemical potential decreases linearly from 1.0 to 0.2 eV, so the chemical potential is expressed by

$$\mu_{c0}(x) = (1.0 - 0.00267x)eV \tag{7.15}$$

Propagation of 3 frequency components, 130, 150 and 180 THz, corresponding to the wavelength of 2.32, 1.99 and 1.66  $\mu\text{m}$ , is simulated. The trapping position is 279.45, 231 and 200.5 nm, respectively. If we incident a broadband SPP wave of which all frequencies have the same amplitude, we will observe broadband light trapping, which is, in other words, rainbow trapping. Figure 7.8 shows the 2 dimensional  $|E|$  field contours of the three frequencies of SPP wave trapped at different locations. Besides broadband frequency trapped, gradient chemical potential distribution structure leads the small momentum mismatching between the incident wave and the eignmode of the local chemical potential and reduces the loss due to the mode evolution.

The other issue arises here is how to release the trapped SPP wave. A. Vakil and N. Engheta proposed a feasible way to tune the chemical potential of the graphene by applied the external gate voltage [30]. In this work, we follow their scheme and make a little modification of the electrode to taper shape to obtain the linear gate voltage distribution along the graphene sheet, and finally dedictate the chemical potential distribution according to the design. Here we still use the chemical potential distribution function of Eq. (7.17), then one can calculate the trapped frequency distribution along the graphene sheet by COMSOL multiphysics. If the incident SPP is composed of a broadband 80 to 350 THz with the same amplitude. Each frequency component is trapped on the graphene sheet according to the chemical potential. The coordinate of the trapped position shifts linearly with the

increasing of the frequency due to the linear function of the chemical potential. When the chemical potential is switched to

$$\mu_{c1}(x) = (1.10 - 0.00267x)eV \quad (7.16)$$

by tuning the external gate voltage. If the impinging frequency span is kept as the same with the above case, The trapped frequency span is from 120 to 350 THz, as shown in Fig. 7.9, which means that the frequency span from 80 to 120 THz transfers from the trapped mode to the propagation mode and leaves the graphene sheet. In other words, this frequency span is released from the graphene sheet as long as the gate voltage increased uniformly along the graphene sheet. Lower frequency of SPP wave is easier to be released due to lower EM energy it carries. Wider frequency span can be released if the chemical potential is higher than  $\mu_{c1}(x)$  uniformly. Furthermore, the releasing speed is relied on how fast the external electric field is established and modified and the speed of the reconstruction of the chemical potential distribution. It should be much faster than that due to the thermal-optical effect [31], even it is possible to get real time control of the group velocity of the SPP wave along the graphene sheet.

It is impossible to get the group velocity equal to zero exactly if the SPP wave suffers loss during propagation [32]. Even it is possible to get the SPP mode vanished before the critical condition is reached. So, estimating the lifetime of the SPP wave at the minimum group velocity becomes significant. The lifetime of the SPP  $\tau_{spp}$  is expressed as  $\tau_{spp} = 1/v_g\alpha$ , where  $v_g$  is the group velocity and  $\alpha$  is the attenuation coefficient of the SPP mode including inherent materials absorption, reflectance, scattering loss and the coupling loss due to the mode momentum mismatching during propagation. However, the graphene monolayer sheet is flatten and smooth is our case, the loss from reflectance and scattering is negligible. Consequently, the total propagation loss which is given by the imaginary part of the propagation constant  $\beta$ .  $v_g$  and  $\alpha$  are calculated from the dispersion relation Eq. (7.9) combining Kubo formula and plotted the lifetime as a function of frequency at various conditions in Fig. 7.10. In the first step, the relaxation time was kept at 0.5 ps, the lifetime as a function of wavelength was calculated at temperature of 270, 300 and 330 K, respectively and the results are plotted in Fig. 7.10a. Interestingly, the lifetime is stable at 3.14 ps in the calculated temperature and frequency spectrum, which is one order higher than other publications [33]. It is rooted from the fact that the electron momentum relaxation time of graphene is orders higher than the counterpart of the noble metals [30]. Furthermore, when we tuned the relaxation time, the lifetime was modified significantly. Figure 7.10b plots the lifetime of 150 THz as a function of relaxation time  $\tau$ , where the lifetime increases linearly from 2.51 ps with a relaxation time of 0.4 ps to 6.29 ps with a relaxation time of 1 ps. So, the lifetime of the trapped SPP wave is mainly determined by the relaxation time, which also determines the metal absorption loss.

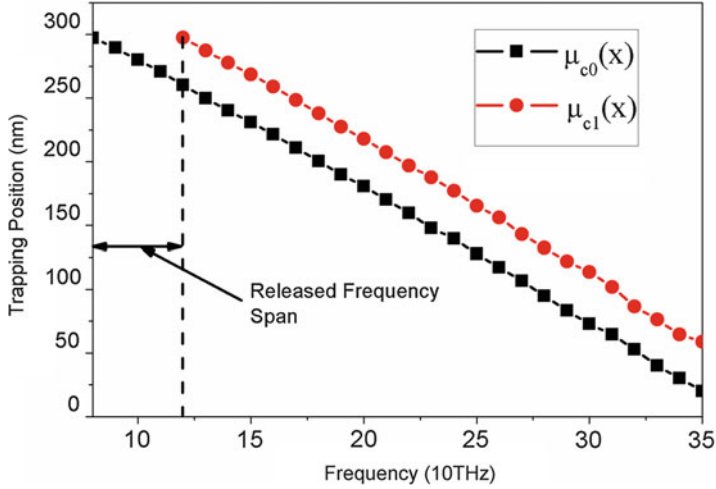


**Fig. 7.9** The trapping position as a function of frequency with various chemical potential distribution of  $\mu_{c0}(x)$  and  $\mu_{c1}(x)$ . The frequency span from 80 to 120 THz transfers from the trapped mode to the propagation mode and leaves the graphene sheet

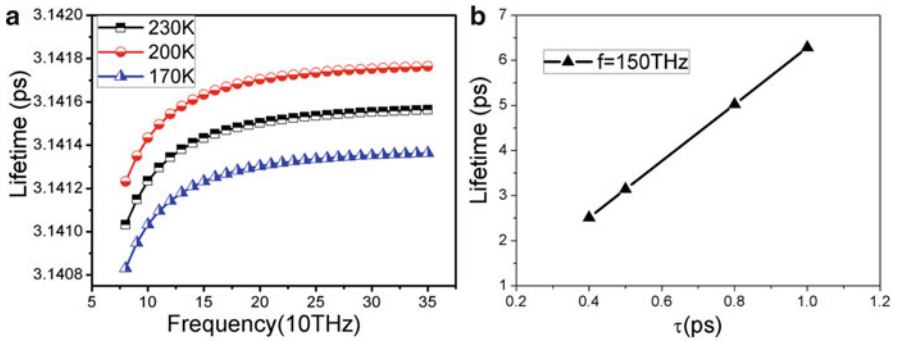


**Fig. 7.10** The lifetime of the trapped plasmons as a function of frequency at a temperature ranged from 170 to 230 K with a relaxation time of 0.5 ps. The lifetime of the trapped plasmon is almost independent from both temperature and frequency. **(b)** The lifetime of the trapped 150 THz plasmon as a function of relaxation time. The lifetime increases linearly with the increasing of the relaxation time

## 7.7 Tunable Plasmonic Whispering-Gallery-Mode Properties of the Graphene Monolayer Coated Dielectric Nanowire and Nanodisks

In order to take full advantages of the WGMs and the high confinements of the SPP waves, dielectric nanowires resonators coated by graphene monolayer instead of noble metals are discussed in this section.

The structure is composed of an infinite long dielectric nanowire coated by graphene with the radius of  $r$ . The length of the nanowire is infinite in the direction perpendicular to the plane of the WGM, so we only consider 2 dimensional pictures of the proposed structure, and the schematic is as shown in Fig. 7.11a. Here,  $n_{air} = 1$  and  $n = 3.45$ .

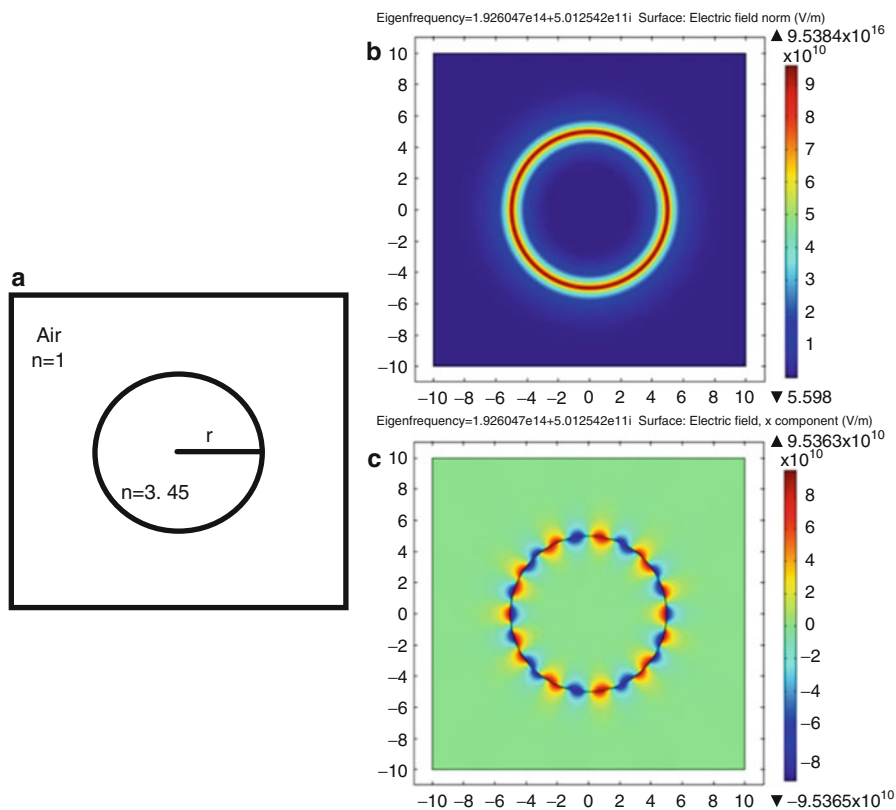


**Fig. 7.11** (a) Schematic diagram of InGaAs nanowire cavity coated with graphene and corresponding COMSOL finite-element computational window.  $r$  indicates the radius of the cavity. The cross-sectional views of the Electrical field (b) ( $E_x$ ) and (c) ( $|E|$ ) distribution of the plasmonic whispering gallery mode with the azimuthal number of 9 at the wavelength of 1.55  $\mu\text{m}$ . The cavity radius is 5 nm and the chemical potential is 0.9 eV



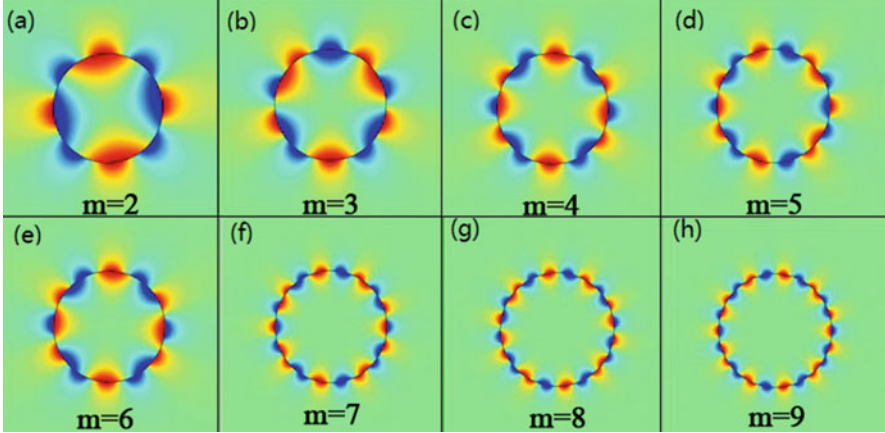


**Fig. 7.12** (a–h) The cross-sectional views of the Electrical field ( $E_x$ ) distribution of the plasmonic whispering-gallery mode with the different azimuthal number ( $m = 2, 3, 4, 5, 6, 7, 8, 9$ ) for the cavity with radius  $r = 5$  nm and chemical potential  $\mu_c = 0.9$  eV

In a dielectric nanowire cavity with  $r = 5$  nm and chemical potential of graphene  $\mu_c = 0.9$  eV, plasmonic WGM with an azimuthal number ( $m$ ) of 9 can be excited at a resonant wavelength of 1550 nm in free space. The electric field ( $E_x$ ) profiles are shown in Fig. 7.11b, c. It is obvious in Fig. 7.11b that the electric field is tightly localized on the surface of the graphene-coated cavity. Also, the  $E_x$  field profiles of various azimuthal numbers from 2 to 9 are revealed in Fig. 7.12a–h.

The electric field becomes tighter and tighter along the circumference of the nanocavity as the azimuthal mode number increases. The  $E_x$  component is anti-symmetric inside and outside the dielectric resonator due to the TM field nature, while the azimuthal number is different in dielectric resonator from that in air region owing to the different refractive index and the non-zero current density in the graphene layer.

According to the eigenvalue analysis section in COMSOL, the eigenvalue is given by  $\beta = \delta - i\gamma$ , which has an imaginary part  $\gamma$  representing the eigen frequency of the resonator, and a real part  $\delta$  representing the damping. The Q factor is defined as

$$Q = \gamma / (2|\delta|), \tag{7.17}$$

For the SPP WGM, besides the quality factor and the azimuthal mode number, another key parameter is the effective mode area  $A_{eff}$ , which is defined by the ratio of a mode’s total energy density per unit length to its peak energy density [34],

$$A_{eff} = \int_{all} W(r) ds / \max[W(r)], \tag{7.18}$$

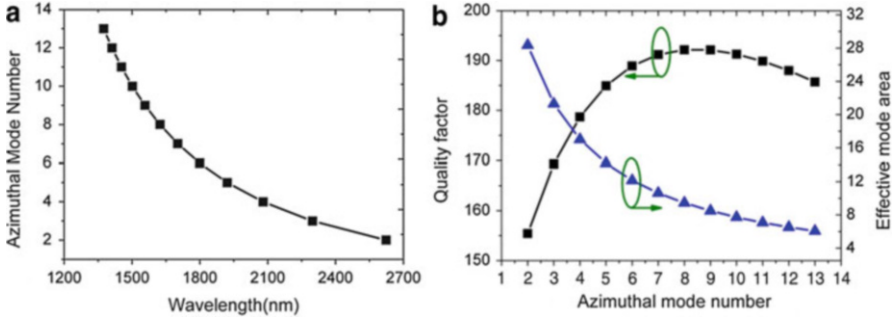


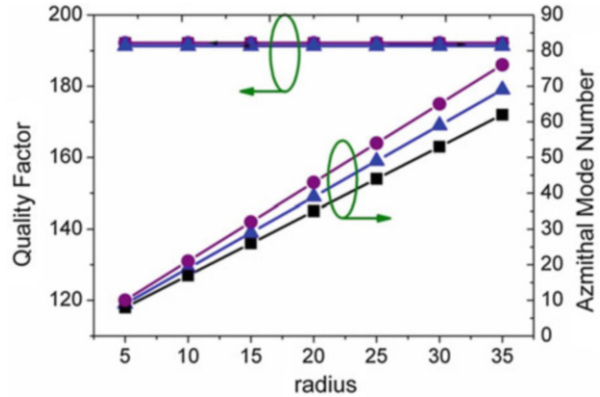
**Fig. 7.13** (a) Azimuthal number as a function of resonant wavelength, (b) Quality factor (black) and effective mode area (blue) as a function of azimuthal number. The radius of the cavity is 5 nm and the chemical potential of graphene is 0.9 eV

where  $W(r) = \frac{1}{2} \text{Re} \left\{ \frac{d[\omega \varepsilon(r)]}{d\omega} \right\} |E(r)|^2 + \frac{1}{2} \mu_0 |H(r)|^2$ , representing the mode energy density.  $|E(r)|^2$  and  $|H(r)|^2$  are the intensity of electric and magnetic fields, respectively,  $\varepsilon(r)$  and  $\mu_0$  are the electric permittivity and magnetic permittivity in the free space, respectively.

Q factors and the effective mode area of the nanowire resonators are calculated as a function of the azimuthal mode number. The radius of the cavity is fixed to  $r = 5$  nm and chemical potential of graphene is kept constant  $\mu_c = 0.9$  eV for comparison. The azimuthal mode number falls down from 13 to 2 with the increasing of the resonance wavelength from 1320 to 2680 nm in Fig. 7.13a. Figure 7.13b plots the Q factor and the effective area as a function of the azimuthal number  $m$ . The Q-factor increases with the increasing the azimuthal number before it reaches the maximum 192.1 at  $m = 8$ , then it falls down slightly when  $m$  keeps going up. However, the effective area reduces monotonously with the increasing of the azimuthal number. This trend means that with the increasing of the azimuthal number, the confinement of the EM field becomes tighter, and it would enhance the EM field density at the interface. In general, the loss of plasmonic resonator is composed of radiation loss and metallic absorption loss. With the increasing of the resonance wavelength, the metallic absorption loss decreases, leading to the Q factor going up. While the resonance wavelength reaches to a certain degree, radiation loss begins rising gradually and even exceeds the reduction of absorption loss, resulting in the falling of Q factor [35]. In the graphene-coated dielectric nanowire structure, the effective mode area is typically smaller than  $3.75 \times 10^{-5} (\lambda_0)^2$  with the resonance wavelength  $\lambda_0$  from 1370 to 2620 nm, much smaller than the conventional optical whispering-gallery mode with the same wavelength.

As a comparison, one can simulate the dielectric nanowire cavity coated by Au and Ag thin films with a thickness of 2 nm. If the resonance wavelength is kept at 1.55  $\mu\text{m}$ , it is found that the quality factor of the Au-coated nanocavity is around 0.33 with an azimuthal mode number of 2, and a radius of 54.5 nm. The quality

**Fig. 7.14** Quality factor and azimuthal number as a function of the radius. The chemical potential is 0.9 eV, and the resonant wavelength is 1.50  $\mu\text{m}$  (black), 1.56  $\mu\text{m}$  (blue), 1.62  $\mu\text{m}$  (purple), respectively



factor of the Ag-coated dielectric nanocavity is 0.14 with the same azimuthal number. For the graphene coated dielectric nanowire cavity, the azimuthal number  $m$  is 109 with the same radius in which the chemical potential is 0.9 eV. This is in stark contrast to the cavity coated by the conventional metal films. Therefore, graphene is much more effective than Au and Ag in achieving a high quality factor for the nanowire resonators.

One can also study the Q factor and the azimuthal number with the change of the radius, when the chemical potential is 0.9 eV. The resonance wavelengths are fixed to 1500 nm (black), 1550 nm (blue) and 1620 nm (purple), respectively. It is shown in Fig. 7.14 that the quality factor is stable at around 192 with all the three resonance wavelengths as the radius increases from 5 to 35 nm, while the azimuthal mode number increases linearly. The absorption loss of the SPP mode decreases with the decreasing of the radius due to the reduction of the travelling distance along the circumference. This effect would result in increasing of the quality factor. On the other hand, the confinement capability of the dielectric cavities without coating degrades as the radius decreases, which would induce a decreasing quality factor. When these two effects balance each other, the total loss during one period along the circumference becomes stable, which finally results in stable quality factors of the various wavelengths and radius. In a SPP WGM cavity, the azimuthal number is roughly satisfied by  $m = 2n_{\text{eff}}\pi r/\lambda_0$ , where  $\lambda_0$  is the wavelength of the EM wave in free space. So it is obvious that the azimuthal mode number is proportional to the radius of the nanowire cavity when the resonant wavelength is kept constant. Nevertheless, if the cavity radius is small, the azimuthal mode number is roughly independent upon the radius and is reverse proportional to the wavelength in high  $m$  region, as shown in Fig. 7.14.

Finally, the quality factors and azimuthal mode numbers of the nanowire cavities are studied with the radius  $r = 5$  nm versus the chemical potential at the resonant wavelength  $\lambda = 1.56 \mu\text{m}$  (blue),  $1.61 \mu\text{m}$  (black), which are shown in Fig. 7.15a. It is obvious that the Q factor increases with the increasing of the chemical potential while the azimuthal mode number decreases. When the chemical potential reduces 0.5 eV from higher level, the azimuthal mode number rises

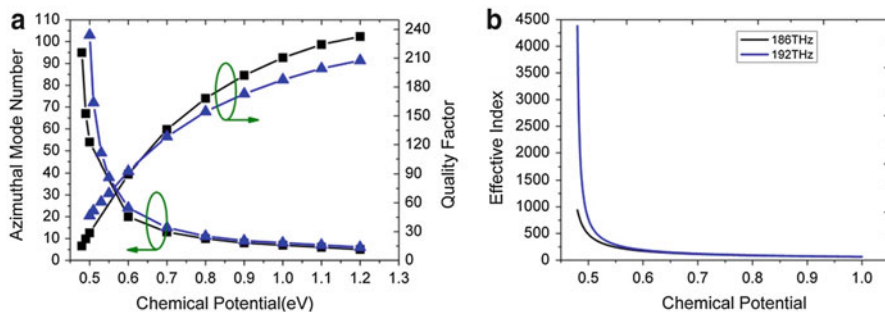


**Fig. 7.15** (a) Quality factor and azimuthal mode number as a function of chemical potential. The radius is 5 nm, (b) The effective index as a function of the chemical potential in flattened graphene. The resonant wavelength is 1.56  $\mu\text{m}$  (blue), 1.61  $\mu\text{m}$  (black), respectively

sharply and the quality factor is less than 20. As it is well known, the propagation loss of graphene supported SPPs is determined by the real parts of the surface conductivity of graphene, and finally determined by the value comparison between the chemical potential  $\mu_c$  and half of the energy of the SPP  $\hbar\omega/2$  [36]. When the chemical potential is much higher than  $\hbar\omega/2$ , the surface conductivity is intraband electron-photon scattering dominated, which results in low propagation loss of SPP mode on graphene. Otherwise, the surface conductivity is interband electron-electron transition dominated and the propagation loss is high which would lead to low quality factor or even no SPP WGM supported in this category of nanocavity [11]. One should make the chemical potential much higher than half energy of the SPP modes to avoid the propagation loss, which would increase the quality factor of the nanocavity, as shown in Fig. 7.15a. A quality factor as high as 235 is achieved when the chemical potential is 1.2 eV. The effective index of SPP wave as a function of the chemical potential of flattened graphene is plotted in Fig. 7.15b. For a certain frequency, as the chemical potential approaches to  $\hbar\omega/2$ , which is around 0.4 eV in our case, the effective index increases drastically, which means the wavelength of the SPP decreases accordingly. The relationship between the effective refractive index and the chemical potential is not exactly the same with that in the WGM case. The trend is adoptable to understand Fig. 7.15a.

## References

1. Grigorenko AN, Polini M, Novoselov KS (2012) Graphene plasmonics. *Nat Photonics* 6:749
2. Wu Y, Lin Y, Bol AA, Jenkins KA, Xia F, Farmer DB, Zhu Y, Avouris P (2011) High-frequency, scaled graphene transistors on diamond-like carbon. *Nature* 472:74
3. Xia F, Farmer DB, Lin Y, Avouris P (2010) Graphene field-effect transistors with high on/off current ratio and large transport band gap at room temperature. *Nano Lett* 10:715
4. Bao Q, Loh KP (2012) Graphene photonics, plasmonics, and broadband optoelectronic devices. *ACS Nano* 6:3677

5. Low T, Avouris P (2014) Graphene plasmonics for terahertz to mid-infrared applications. *ACS Nano* 8:1086
6. Wang J, Lu W, Liu J, Cui T (2015) Digital metamaterials using graphene. *Plasmonics* 10:1141
7. Chen PY, Alù A (2011) Atomically thin surface cloak using graphene monolayers. *ACS Nano* 5:5855
8. Bao Q, Zhang H, Wang Y, Ni Z, Yan Y, Shen ZX, Loh KP, Tang DY (2009) Atomic-layer graphene as a saturable absorber for ultrafast pulsed lasers. *Adv Funct Mater* 19:3077
9. Bao Q, Zhang H, Wang B, Ni Z, Haley C, Lim YX, Wang Y, Yuan DT, Loh KP (2011) Broadband graphene polarizer. *Nat Photonics* 5:411
10. Kanade P, Yadav P, Kumar M, Tripathi B (2015) Plasmon-induced photon manipulation by Ag nanoparticle-coupled graphene thin-film: light trapping for photovoltaics. *Plasmonics* 10:157–164
11. Jablan M, Buljan H, Soljačić M (2009) Plasmonics in graphene at infrared frequencies. *Phys Rev B* 80:245435
12. Farhat M, Rockstuhl C, Bağcı H (2013) A 3D tunable and multi-frequency graphene plasmonic cloak. *Opt Express* 21:12592
13. Dash JN, Jha R (2015) On the performance of graphene-based D-shaped photonic crystal fibre biosensor using surface plasmon resonance. *Plasmonics* 10:1123
14. Christensen J, Manjavacas A, Thongrattanasiri S, Koppens FHL, de García Abajo F (2012) Graphene plasmonic waveguiding, and hybridization in individual paired nano-ribbons. *ACS Nano* 6:431
15. He S, Zhang X, He Y (2013) Graphene nano-ribbon waveguides of record small mode area and ultra-high effective refractive indices for future VLS. *Opt Express* 21:30664
16. Brar VW, Jang MS, Sherrott MJ, Atwater H (2013) Highly confined tunable mid-infrared plasmonics in graphene nanoresonators. *Nano Lett* 13:2541
17. Zhu X, Yan W, Mortensen N, Xiao S (2013) Bends and splitters in graphene nanoribbon waveguides. *Opt Express* 21:3486
18. Li H, Wang L, Liu J, Huang Z, Sun B (2014) Tunable, mid-infrared ultra-narrowband filtering effect induced by two coplanar graphene stripes. *Plasmonics* 9: 1239–1243
19. Danaeifar M, Granpayeh N, Mohammadi A, Setayesh A (2013) Graphene-based tunable terahertz and infrared band-pass filter. *Appl Opt* 52:E68
20. Cheng H, Chen S, Yu P, Li J, Deng L, Tian J (2013) Mid-infrared tunable optical polarization converter composed of asymmetric graphene nanocrosses. *Opt Lett* 38:1567
21. Sensale-Rodriguez B, Yan R, Kelly M, Fang T, Tahy K, Hwang W, Jena D, Liu L, Xing H (2011) Broadband graphene terahertz modulators enabled by intraband transitions. *Nat Commun* 3:1787
22. Yao Y, Kats MA, Genevet P, Yu N, Song Y, Kong J, Capasso F (2013) Broad electrical tuning of graphene-loaded plasmonic antennas. *Nano Lett* 13:1257
23. Liu H, Sun S, Wu L, Bai P (2015) Optical near-field enhancement with graphene bowtie antennas. *Plasmonics* 9:845
24. Chen L, Zhang T, Li X, Wang G (2013) Plasmonic rainbow trapping by a graphene monolayer on a dielectric layer with a silicon grating substrate. *Opt Express* 21:28628
25. Nikitin AY, Low T, Martin-Moreno L (2014) Anomalous reflection phase of graphene plasmons and its influence on resonators. *Phys Rev B* 90:041407
26. Efetov DK, Kim P (2010) Controlling electron-phonon interactions in graphene at ultrahigh carrier densities. *Phys Rev Lett* 105:256805
27. Dean CR, Young AF, Meric I, Lee C, Wang L, Sorgenfrei S, Watanabe K, Taniguchi T, Kim P, Shepard KL, Hone J (2010) Boron nitride substrates for high-quality graphene electronics. *Nat Nanotechnol* 5:722
28. Yan H, Low T, Zhu W, Wu Y, Freitag M, Li X, Guinea F, Avouris P, Xia F (2013) Damping pathways of mid-infrared plasmons in graphene nanostructures. *Nat Photonics* 7:394
29. Lindquist NC, Nagpal P, Lesuffleur A, Norris DJ, Oh SH (2010) Three-dimensional plasmonic nanofocusing. *Nano Lett* 10:1369

30. Vakil A, Engheta N (2010) Transformation optics using graphene. *Science* 332:1291–1294, 2011
31. Gan Q, Ding YJ, Bartoli FJ (2009) “Rainbow” trapping and releasing at telecommunication wavelengths. *Phys Rev Lett* 102:56801
32. Reza A, Dignam MM, Hughes S (2009) Can light be stopped in realistic metamaterials? *Nature* 455(7216):E10–E11
33. Chen L, Wang GP, Gan Q, Bartoli FJ (2009) Trapping of surface-plasmon polaritons in a graded bragg structure: frequency-dependent spatially separated localization of the visible spectrum modes. *Phys Rev B* 80:161106
34. Falk AL, Koppens FH, Chun LY, Kang K, de Snapp Leon N, Akimov AV, Jo M, Lukin MD, Park H (2009) Near-field electrical detection of optical plasmons and single-plasmon sources. *Nat Phys* 5:475
35. Chen Y, Zou C, Hu Y, Gong Q (2013) High-Q plasmonic and dielectric modes in a metal-coated whispering-gallery microcavity. *Phys Rev A* 87:23824
36. Hanson GW (2008) Dyadic Green’s functions and guided surface waves for a surface conductivity model of graphene. *J Appl Phys* 103:64302